Artificial Space Weathering to Mimic Solar Wind Enhances the Toxicity of Lunar Dust Simulants in Human Lung Cells

J. H. M. Chang[1], Z. Xue[1], J. Bauer[1], B. Morrow[1], D. Hendrix[2,3], T. Catalano[2], J. A. Hurowitz[2], H. Nekvasil[2], and B. Demple[4]

[1]Department of Pharmacological Sciences, Renaissance School of Medicine, Stony Brook University, NY 11794, USA

[2]Department of Geosciences, Stony Brook University, NY 11794, USA

[3]National High Magnetic Field Laboratory, Florida State University, Tallahassee, FL 32310, USA

[4]Departments of Pharmacological Sciences and of Radiation Oncology, Renaissance School of Medicine, Stony Brook University, NY 11794, USA

Corresponding author: Bruce Demple (bruce.demple@stonybrook.edu)

Key Points:

- Lunar dust remains a potential threat to the health of astronauts in the Artemis Program, since they will carry out regular missions to the Moon with extended stays.
- Lunar dust simulants chemically reduced to mimic “space weathering” by solar wind enhanced all of the toxic effects of these materials.
- Toxicity in cells exposed to the simulants was newly investigated with probes for mitochondrial function, real-time O_2 consumption, and nuclear DNA damage.
- Antioxidant supplementation of the cells decreased all the toxic endpoints examined, pointing to a pivotal role for free radicals in dust-induced toxicity.

Abstract

During NASA's Apollo missions, inhalation of dust particles from lunar regolith was identified as a potential occupational hazard for astronauts. These fine particles adhered tightly to spacesuits and were brought accidentally into the living areas of the spacecraft. Apollo astronauts reported that exposure to the dust caused intense respiratory and ocular irritation. This problem is a potential challenge for the Artemis Program, which aims to return humans to the Moon for extended stays in this decade. Since lunar dust is "weathered" by space radiation, solar wind, and the incessant bombardment of micrometeorites, we investigated whether treatment of lunar regolith simulants to mimic space weathering enhanced their toxicity. Two such simulants were employed in this research, Lunar Mare Simulant-1 (LMS-1), and Lunar Highlands Simulant-1 (LHS-1), which were applied to human lung epithelial cells (A549). In addition to pulverization, previously shown to increase dust toxicity sharply, the simulants were exposed to hydrogen gas at high temperature as a proxy for solar wind exposure. This treatment further increased the toxicity of both simulants, as measured by the disruption of mitochondrial function, and damage to DNA both in mitochondria and in the nucleus. By testing the effects of supplementing the cells with an antioxidant (N-acetylcysteine), we showed that a substantial component of this toxicity arises from free radicals. It remains to be determined to what extent the radicals arise from the dust itself, as opposed to their active generation by inflammatory processes in the treated cells.

Plain Language Summary

With the Artemis program, humans will soon return to explore the Moon. However, lunar surface dust has toxic potential that must be assessed in order to clarify short-term and long-term health risks for Artemis astronauts. Numerous studies indicate that Moon dust has chemical and physical properties that may strongly affect dust toxicity. Unlike terrestrial dust, lunar regolith experiences "space weathering" under a vacuum, including the effects of solar wind, which further modifies the bulk and surface properties of this dust. In this work, we used two lunar dust simulant materials that were chemically treated to mimic the effects of space weathering. This treatment strongly increased all the toxic effects of both simulants: cell killing, mitochondrial dysfunction, and damage to DNA. Other experiments point to free radicals as a significant component of these effects. Future work will address whether these radicals arise from the simulants themselves or are generated by cellular activity.

1 Introduction

1.1 Dust exposure and pulmonary disease

Occupational exposure to silica dust in mines underlies the development of diseases such as silicosis in humans [*Hessel et al.*, 1988; *Hnizdo and Vallyathan*, 2003; *Hnizdo et al.*, 1997; *Merget et al.*, 2002]. Other types of fine particles also exert toxicity and cause chronic pulmonary disease [*Hsu et al.*, 2018; *Hu et al.*, 2016; *Medina-Reyes et al.*, 2015; *Skuland et al.*, 2020]. The properties of lunar dust suggest it to be a potential risk for humans if they are exposed [*Linnarsson et al.*, 2012].

1.2 Lunar dust

As shown in previous studies [*Cain*, 2010; *Loftus et al.*, 2008; *Wagner*, 2006], Moon dust is highly reactive because of space weathering, including exposure to intense UV

light, ionizing radiation, solar wind, and micrometeorite bombardment. The dust particles become finer, more jagged, and more reactive as a result of this weathering; indeed, lunar dust adhered strongly to spacesuits, thus bringing the material into the living areas and causing respiratory and other irritations [*Gondhalekar et al.*, 2020].

1.3 Our study

To build on our previous work [*Caston et al.*, 2018; *Hendrix et al.*, 2019], here we have applied new experimental techniques to assess the toxic effects of lunar dust on cells. New lunar dust simulants were used as better mimics of the composition and properties of lunar regolith. We mimicked solar wind effects artificially by exposing the simulants to strongly reducing conditions. The possible contribution of free radicals and reactive oxygen species (ROS) [*Hendrix et al.*, 2019; *Linnarsson et al.*, 2012; *Pohlen et al.*, 2022] was addressed by testing whether antioxidant supplementation of the cells affected the various toxic endpoints.

2 Materials and Methods

2.1 Cell Culture

Human lung alveolar epithelial cells (A549) were cultured at 37°C in Ham's F12-K (Kaighn's) nutrient medium (Gibco #21127022) supplemented with 10% fetal bovine serum (Corning #MT35010CV) and an antibiotic/antimycotic mix diluted 100-fold from the commercial stock solution (Sigma-Aldrich #A5955100-ML) [*Caston et al.*, 2018]. For most of the experiments presented here, at least 12 h before, cells in supplemented medium were seeded at 8×10^5 per well in 6-well plates (Corning #3516). Dust exposures (1 h) were conducted in serum-free medium. For pretreatment with N-acetylcysteine (NAC), pilot experiments explored concentrations of 0.05-5 mM NAC for 2-24 h based on published studies [*Mitsopoulos and Suntres*, 2011] for protection of A549 cells against H_2O_2 toxicity. Based on those results, a standard protocol was established: cells were incubated in growth medium freshly supplemented with 5 mM NAC for 24 h before a toxic challenge, with NAC supplementation continued in the post-challenge incubation.

2.2 General Preparation of Simulant Materials

The Lunar Mare Simulant-1 (LMS-1) and the Lunar Highlands Simulant-1 (LHS-1) used in this study were purchased from EXOLITH Lab (532 S Econ Cir, Oviedo, FL 32765, USA). Both are composed of terrestrial minerals and glass, and have higher Na and K, and lower Fe, Mg, and Ca contents than typical lunar regolith. To simulate the finest regolith size fraction (<10μm) the simulants were sieved through 63-μm mesh, and crushed in a Retsch PM 100 planetary agate ball mill down to an average grain size <10 μm and including <1 μm particles. Surface areas of samples were measured by gas adsorption using ultra high purity nitrogen gas via six-point Brunauer-Emmett-Teller theory on a NOVA-2000 BET analyzer as described [*Hendrix et al.*, 2021]. The resulting material was fine powder composed of angular mechanically crushed grains. While this simulates some physical properties of lunar regolith, it does lack agglutinates, which are small clods of dust particles welded together by silicate glass.

Synthetic olivines with varying iron:magnesium ratios were made from oxide components, SiO_2, MgO, Fe_3O_3, and Fe(0) metal. The components were first measured out in the correct ratios for olivine, including a correct ratio of ferric to metallic iron. The oxides were mixed for 2 h in an automatic mortar and pestle with ethanol. After grinding, the mix powder was dried, and the sample was prepared for reaction by packaging into an Ag foil tube inside a silica tube. Once the tube was packed, a capillary was drawn in the silica tube, and the sample was put under vacuum. Before removing the sample from the vacuum line, it was dried by heating to 800°C for 15 min, with the Fe sponge O_2-getter heated to ~600°C. After cooling, the sample was separated from the remainder of the tube by melting at the capillary. After preparation, the samples reacted at 900ºC for 2 weeks in a platinum wound horizontal furnace. Following this step, the samples were tested for purity using powdered X-ray diffraction. Most samples required a second 2-week reaction at 900°C and were again checked for purity using powdered X-ray diffraction.

2.3 Artificial Space Weathering and Processing of Simulant Materials

Pulverization of simulant materials (to mimic some effects of impact gardening) substantially increases their toxicity [*Caston et al.*, 2018]. To mimic the effect of solar wind and micrometeorite bombardment on the dust properties, ground simulants were reduced in hydrogen gas at 900°C based on a published method [*Allen et al.*, 1994]. This treatment resulted in changes in the physical and chemical properties of the material, including the reduction in apparent grain size, and the decreased surface area of the particles (Fig. 1) [*Allen et al.*, 1994]. After initial processing, all the materials were stored under vacuum, and immediately before use, they were re-ground for 3 min with a mortar and pestle (freshly cleaned with 70% ethanol).

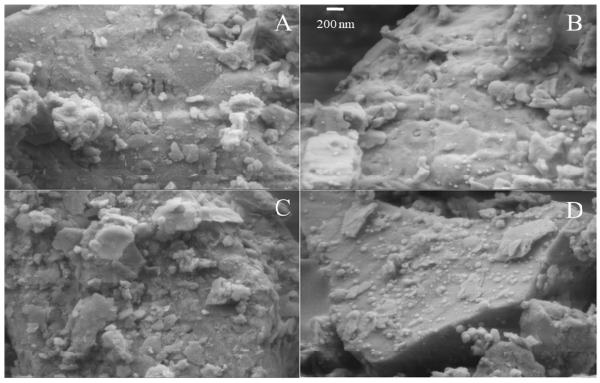

Figure 1. Close up SEM images of lunar simulants before and after reduction treatment. All images have the same scale. (A) LHS-1, (B) LHS-1 after reduction, (C) LMS-1, (D) LMS-1 after reduction. Reduced simulants show the development of Fe nanoparticles on grain surfaces.

2.4 Cell Treatment and Survival Assay

After weighing out the simulant samples, they were ground and added directly to cells in serum-free cell culture medium, followed by a 1-h incubation at 37°C. The cells were then rinsed with sterile phosphate-buffered saline (137 mM NaCl, 2.7 mM KCl, 10 mM Na_2HPO_4, 1.8 mM KH_2PO_4) to wash most dust particles away. Following dust exposure, the cells were incubated another 24 h in serum-containing growth medium. After removal of the medium, the cells were recovered by the addition 0.5 mL of a solution containing 0.25% trypsin and 2.21 mM EDTA (Corning# 25-053-Cl). After 3 min at 37 °C, 0.5 mL of serum-supplemented medium was added to neutralize the trypsin. After gently mixing, 10-µL aliquots of cell solution were mixed with 10-µL aliquots of 0.4% trypan blue dye (Sigma #T8154). The stained cell

153 samples were counted on a hemocytometer under microscope, with the blue-stained
154 cells scored as dead [*Strober*, 2001]. The control count was normalized to 100%
155 [*Caston et al.*, 2018].

156 2.5 MitoSOX Red

157 The protocol was based on a previous study [*Wojtala et al.*, 2014]. A 5 mM stock
158 solution of MitoSOX Red Mitochondrial Superoxide Indicator (Invitrogen #M36008)
159 was prepared in dimethyl sulfoxide and stored at 20 ℃. Immediately before use with
160 the cell samples, the MitoSOX Red stock was diluted to 0.5 μM with Hank's balanced
161 salt (HBSS) solution: 140 mM NaCl, 5 mM KCl, 1 mM $CaCl_2$, 0.4 mM
162 $MgSO_4 \cdot 7H_2O$, 0. 5 mM $MgCl_2 \cdot 6H_2O$, 0. 3 mM Na_2HPO_4, 0.4 mM KH_2PO_4, 6 mM
163 glucose, 4 mM $NaHCO_3$ [*Laboratories*, 2006]. Freshly reground lunar regolith
164 simulants were added directly to each well. After the exposure, the cells were washed
165 twice with HBSS, MitoSOX solution was added, and the incubation continued for 1.5
166 h. The cells were then washed twice with HBSS buffer. Fluorescent microscope
167 images were acquired using a BioTek Lionheart Imager. The cells were then released
168 by trypsinization for 3 min, which was stopped by adding serum-containing medium.
169 The cells were then collected by centrifugation at 600×g for 5 min, and resuspended
170 with HBSS buffer at $8x10^4$ cells per mL. To measure total fluorescence, a 100-μL
171 aliquot of the cell suspension was placed in each well of a 96-well plate (Thermo
172 Scientific #265301). Quantification of the fluorescence was done using a Molecular
173 Devices SpectraMax M5 Microplate Reader, with excitation at 510 nm, and emission
174 measured at 580 nm. The background fluorescence was subtracted, and the controls
175 were normalized to 1.

176 2.6 Real-time Detection of Oxygen Consumption Rate

177 The RESIPHER device (Lucid Scientific, Atlanta, GA) allows the real-time detection
178 of oxygen consumption by cells, with multiple samples measured simultaneously in
179 96-well plates (Thermo Scientific #167852) and for extended times. For these
180 experiments, aliquots of 2×10^5 cells per well were seeded 24 h prior to treatment and
181 incubated at 37°C; all samples were set up in four replicates. The O_2 -sensing lids are
182 placed after cells are settled in each well. Non-reduced or reduced LMS-1, suspended
183 in 200 μL of serum-free cell culture medium, was applied at 0.05, 0.1, or 0.15 mg/cm^2
184 into individual wells. As a positive control for mitochondrial disruption, the Complex
185 III inhibitor antimycin A was added at 20 μM. During the exposure to antimycin A or
186 the dust particles, the O_2-sensing lid was temporarily replaced with a normal lid.
187 After a 1-h challenge with LMS-1, serum-supplemented medium was added in the
188 wells, and the O_2-sensing lid was added to the plate again. The oxygen sensors will
189 continuously monitor the oxygen concentration in the culture media with
190 measurements taken automatically every 36 sec for every well. As the cells consume
191 oxygen, an oxygen concentration gradient is generated, with the rate of O_2
192 consumption calculated by the software continuously up to 72 h in our experiments.
193 The data were analyzed based on instructions from the manufacturers using GraphPad
194 Prism.

195 ## 2.7 Quantitative Polymerase Chain Reaction (PCR) Assay

196 For this analysis, immediately after a 1-h challenge with dust or other agents, total
197 cellular DNA was extracted using the QIAGEN 20/G DNA extraction kit (Qiagen
198 #10223). DNA concentrations were quantified using a NanoDrop ND-1000
199 Spectrophotometer. The PCR assay protocols here were slightly revised from
200 previous protocols [*Ayala-Torres et al.*, 2000; *Caston et al.*, 2018; *Furda et al.*, 2014]
201 DNA. For "long" mitochondrial PCR (amplifying about half of the mitochondrial
202 DNA molecule, 15 ng of DNA template was mixed with LongAmp buffer and 100
203 U/mL of LongAmp Taq polymerase (New England Biolabs #M0323S), 300 μM each
204 of the four deoxynucleotide triphosphates, and 400 nM each of the forward and
205 reverse primers (See Table 1), in a total volume of 50 μL. The thermocycler was set
206 for 3 min at 95°C for the initial denaturation, followed by 20 cycles of 15 s at 95°C
207 for denaturation and 9 min at 60 °C for primer annealing and extension, and a 21st
208 cycle with a final extension at 65°C for 10 min. For the "short" mitochondrial PCR,
209 25 ng of DNA template was mixed with ThermoPol buffer and 25 U/mL of
210 ThermoPol Taq polymerase (New England Biolabs #M0267S), 150 μM each of the
211 four deoxynucleotide triphosphates, and 1 μM each of the forward and reverse
212 primers (See Table 1), in a total volume of 50 μL. The thermocycler program for
213 short PCR was 2 min at 95°C for the initial denaturation, followed by 22 cycles of 15
214 s at 95°C for denaturation, 30 s at 56°C for annealing, 1 min at 68°C for extension,
215 and finished with a final extension at 68°C for 5 min. The long PCR product is 8,843
216 base pairs, and the short PCR product is 222 base pairs. The PCR products were
217 quantified using the Picogreen reagent (Thermo-Fisher P11496) to detect double-
218 stranded DNA, with the fluorescent signals acquired from a Molecular Devices
219 SpectraMax M5 Microplate Reader. Since the long PCR reaction has a much greater
220 chance of encountering a lesion in the template than is the case for the short PCR
221 reaction, the ratio of their products reflects the DNA damage level. The controls were
222 normalized to a ratio of 1.

223 ## 2.8 Alkaline Comet Assay

224 The alkaline comet assay was used to detect both single-strand breaks and double-
225 strand breaks in DNA in the cell nucleus. Our protocol was adapted from published
226 studies [*Muruzabal et al.*, 2021; *Nowsheen et al.*, 2012; *Tice et al.*, 2000]. Following
227 dust treatment and trypsinization, the recovered cell number was estimated using a
228 hemocytometer, then mixed with 1% low-melting-point agarose gel (SeaPlaque GTG
229 Agarose #50110) at 37°C. The agarose-cell suspension was then placed on warmed
230 glass microscope slides (180 μL per slide), which were cooled to room temperature to
231 allow the gel to set. Lysis buffer with concentration of 2.5 M NaCl, 0.1 M
232 $Na_2EDTA{\cdot}H_2O$, and 0.01 M tris is first prepared, and then adjusted to pH=10 with
233 NaOH with final concentration of 0.03 M L-Lauroylsarcosine sodium salt stirred in
234 the lysis buffer. After the gels had set, they were incubated in the mixture of 66.75
235 mL lysis buffer, 7.5 mL DMSO, and 0.75 mL of Triton X-100 at 4°C for 1 h. The
236 slides were then transferred to a neutralizing buffer containing 4 M tris (adjusted to
237 pH=7.5 with NaOH before use) to remove the lysis buffer, then incubated with the
238 alkaline electrophoresis buffer containing 0.3 M NaOH and 1 mM $Na_2EDTA{\cdot}H_2O$.
239 The slides were subjected to electrophoresis at 20 V/cm for 20 min. Following

electrophoresis, the slides were dried overnight at room temperature, then stained with 0.5 mL SYBR Gold (Invitrogen™ #S11494) for microscopic visualization. Images of the stained cells were obtained using a Nikon E400. Images were processed to remove auto-fluorescent signals of the dust particles. At least 100 cells were then analyzed for each sample through OpenComet as described [*Gyori et al.*, 2014].

3 Results

3.1 Cell Viability After Exposure to LMS-1 and LHS-1

We tested the possible contribution of solar wind-mediated space weathering to simulant toxicity by comparing the cytotoxicity of untreated and artificially reduced simulants. Cell survival was scored with the trypan blue exclusion assay (see Materials and Methods). Non-reduced LMS-1 (Fig. 2A) and LHS-1 (Fig. 2B) were both strongly cytotoxic even at the lowest exposure (0.5 mg/cm^2). Importantly, the cytotoxicity of both materials was strongly enhanced by the reducing treatment (Fig. 2A, B).

To test the possible role of free radicals and oxidative damage in the cytotoxicity of the simulants, we supplemented the cells with NAC, which both is an antioxidant itself and boosts the capacity of cellular reducing pathways [*Ates et al.*, 2008]. Pilot experiments determined the effective level of the antioxidant, with the best protection achieved using 5 mM NAC supplementation 60 min before dust exposure, and the continued presence of the antioxidant after the exposure. This NAC supplementation increased cell survival both for LMS-1 (Fig. 2C) and for LHS-1 (Fig. 2D) exposures of 0.5 mg/cm^2.

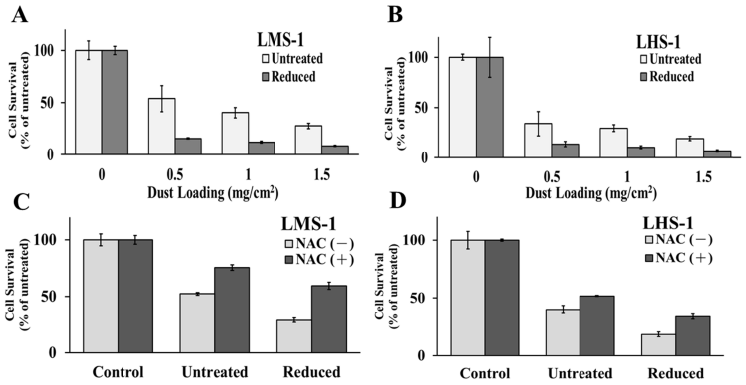

Figure 2. Viability of human lung alveolar epithelial cells exposed to LMS-1 or LHS-1 and effect of artificial space weathering. A549 cells were treated for 1 h with the indicated amounts of freshly-ground simulants (**A**) LMS-1 or (**B**) LHS-1, the dust removed, and growth medium replaced. After a subsequent incubation for 24 h, viability was scored by trypan blue exclusion. Where indicated, N-acetylcysteine (NAC) was added 24 h before the exposure to (**C**) LMS-1 or (**D**) LHS-1 at 0.5 mg/cm^2. The p values were all <0.05: between the untreated and reduced materials in A and B, and in C and D between NAC-supplemented and non-supplemented medium, as well as between nontreated and reduced simulants.

Given the likely role of the particle surface in toxicity [*Pohlen et al.*, 2022], we computed the initial rates of cell-killing as a function of particle surface area. That computation (Table 2) also confirmed (i) that LHS-1 was more toxic than LMS-1, (ii) that the reducing treatment significantly enhanced the toxicity of both types of simulants, and (iii) that the antioxidant supplementation increased cell survival in all cases.

The differing toxicity of LMS-1 and LHS-1 presumably reflects their differing compositions (Table 3) [*Hendrix et al.*, 2019]. Iron-containing minerals may be contributors to oxidant production and toxicity [*Hendrix et al.*, 2019], bearing in mind

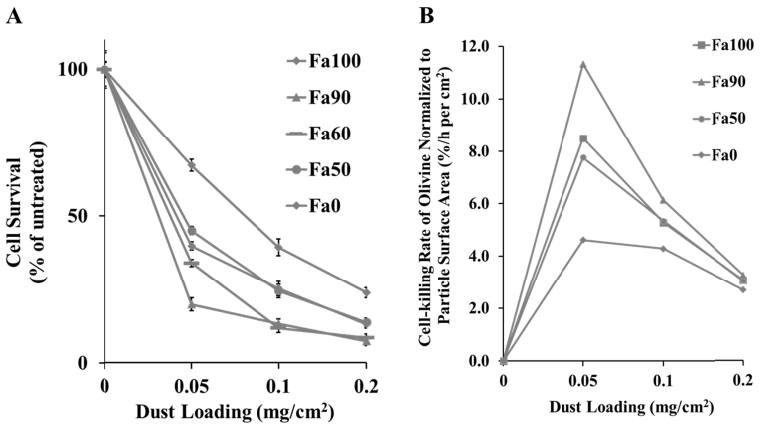

Figure 3. Viability of A549 cells exposed to olivine of differing Fe:Mg composition (Fa100, Fa90, Fa60, Fa50, and Fa0). **A**, Freshly-ground samples were added to A549 cells for 1 h; after dust removal and restoration of growth medium, viability was scored 24 h later by trypan blue exclusion. The p values were <0.05 for all comparisons except Fa50 vs. Fa100. **B**, Cell killing rate as a function of dust surface area.

that this aspect of the materials is unlikely to be the sole determinant of toxicity. To address this point, we used olivine (a silicate mineral found in lunar dust) with different Fe/Mg ratios, varying the proportions of Fe_2SiO_4 (Fayalite component) to Mg_2SiO_4 (forsterite component) in the mineral from 100:0 to 0:100 (Fa100 to Fa0 [*Heiken et al.*, 1991]). Olivine was chosen due to its availability and its high affinity to generate hydroxyl radical in solution [*Hendrix et al.*, 2019; *Hendrix et al.*, 2021]. The results (Fig. 3A) showed some dependence on Fe content, except for Fa100, which appeared less toxic than Fa90 or Fa60, and about the same as Fa50. However, each of these simulants has a different particle surface area [*Hendrix et al.*, 2021]. When the surface area was taken into account, the results showed that Fa100 was twice as cytotoxic as Fa90 or Fa50, and at least 10-fold more toxic than Fa0 (Fig. 3B). The differences were most evident for the lowest level of dust exposure, which was expected given the low survivals seen for exposure to higher amounts of dust (Fig. 3A). The result is consistent with iron being a significant component of the cell-killing activity of the simulants.

3.2 Mitochondrial DNA Damage After Exposure to LMS-1 and LHS-1

Our previous study [*Caston et al.*, 2018] showed dust-dependent damage to mitochondrial DNA by other lunar dust simulants. For the new materials, we used the same assay based on PCR, in which DNA damage is reported as a diminished product signal [*Ayala-Torres et al.*, 2000; *Furda et al.*, 2014]. The integrity of mitochondrial DNA was decreased immediately after a 1-h exposure to non-reduced LMS-1 or non-reduced LHS-1, with the latter showing higher toxicity (Fig. 4A). As seen for cytotoxicity, damage to mitochondrial DNA was strongly enhanced by the artificial space weathering, but with the results for the two simulants not significantly different (Fig. 4A). Again, in parallel to the cell survival results, mitochondrial DNA damage was diminished by the antioxidant supplementation for both simulants in the reduced form (Fig. 4B). In summary, the reduced materials caused greater damage to

322 mitochondrial DNA, and NAC supplementation gave a consistent protective effect.

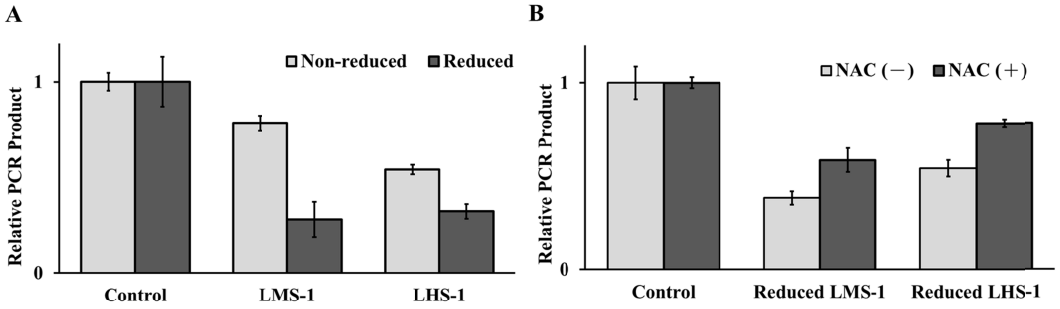

Figure 4. Simulant-induced mitochondrial DNA damage. **A**, Freshly-ground LMS-1 or LHS-1, with or without prior reducing treatment, were added at 1.5 mg/cm^2 to cells in 6-well plates, and after 1 h, total DNA was immediately extracted for the PCR assay. **B**, Protection by antioxidant supplementation. Reduced and freshly-ground reduced LMS-1 or LHS-1 were added after NAC pretreatment where indicated, and after 1 h, total DNA was immediately extracted for the PCR assay. The p value for all pairwise comparisons was <0.05.

323

324 ## 3.3 Mitochondrial Function after Exposure to LMS-1 and LHS-1

325 The observed rapid damage to mitochondrial DNA poses the question of whether
326 mitochondrial function was affected. To probe this question, we used the cationic dye
327 MitoSOX Red, which enters mitochondria and forms a fluorescent signal after
328 reaction with superoxide, the initial product of disrupted respiratory chains in these
329 organelles [*Kowaltowski et al.*, 2009]. As seen for the other measures, both LMS-1
330 and LHS-1 caused significant mitochondrial disruption within the 1-h exposure (Fig.
331 5AB). Mitotoxicity was enhanced for the reduced compared to non-reduced materials.
332 And once again, the mitotoxicity was in all cases significantly diminished by
333 antioxidant supplementation. Some examples of increased MitoSOX Red staining in
334 dust-treated cells are shown in Fig. 5C. These results show that exposure to lunar dust
335 simulants can rapidly damage mitochondrial DNA and disrupt mitochondrial

function.

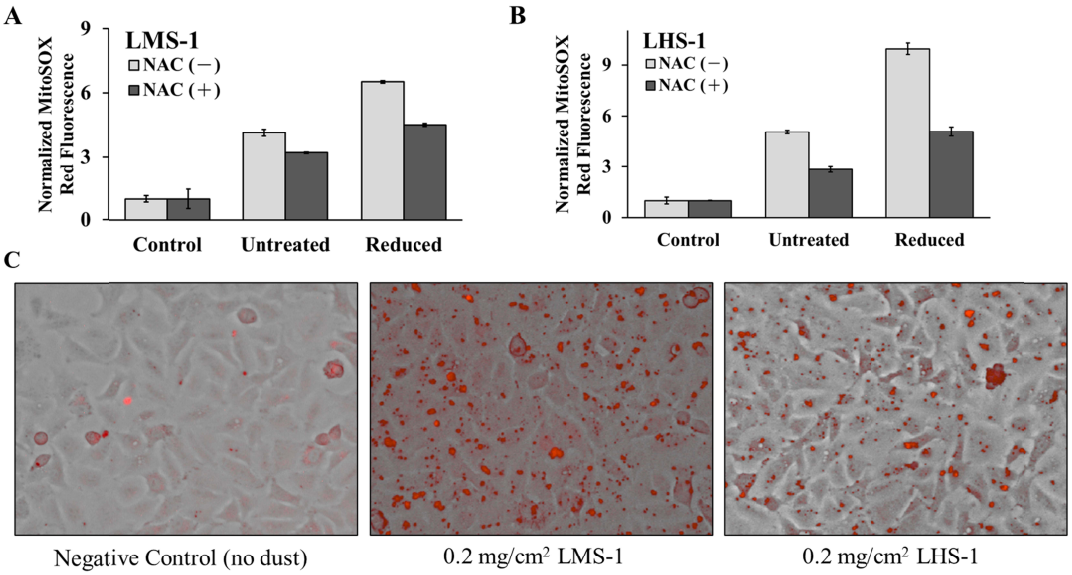

Figure 5. MitoSOX Red fluorescence after exposure to simulants. Freshly-ground LMS-1 and LHS-1 were added at 0.5 mg/cm^2 to A549 cells for 1 h and the dust removed, followed by a 1.5-h incubation with the MitoSOX Red. Fluorescent signals were then recorded for quantification (**A, B**). Examples of MitoSOX Red staining are shown in **C**. The p value between groups is less than 0.05.

3.4 Real-time Oxygen Consumption in Cells After Exposure to LMS-1

Mitochondria generate energy in the form of ATP, largely dependent on the consumption of oxygen [*Kowaltowski et al.*, 2009]. Given the rapid disruption of mitochondrial function in dust-exposed cells, we tested a more direct technique for monitoring the activity of the organelle. This approach monitored O_2 consumption continuously in multiple samples over several days (see Materials and Methods). Pilot experiments established that we would detect mitotoxicity caused by amounts of dust 10-fold lower than needed for the other assays. Fluctuations of O_2 consumption during the first ~12 h are due to the time needed for equilibration with the oxygen present in the incubation chamber. Untreated cells continued to consume O_2 at a rate that increased over the first 48 h as cell proliferation continued, leveling off as the cells multiplied to fill the test well area. Even the lowest level of *non-reduced* LMS-1 dampened O_2 metabolism and partly suppressed the increase over 72 h (Fig. 6). Higher levels of non-reduced LMS-1 suppressed all O_2 consumption during the first 12 h after exposure and prevented any significant recovery out to 72 h, with the effect of 0.15 mg/cm^2 as profound as that of the positive control antimycin A, which blocks the respiratory chain immediately before the O_2-consuming step (Fig. 6). Reduced LMS-1 proved much more mitotoxic than the non-reduced materials, with immediate effect and little to no recovery at even the lowest level of exposure (Fig. 6). The reduced materials all produced an early and transient spike in apparent O_2 consumption, but that appears to be an artifact which possibly reflects the generation of ROS by the particles, thus leading to oxygen consumption. It is clear, however, that this approach allows dust toxicity to be revealed with greater sensitivity and over

a more extended period after exposure.

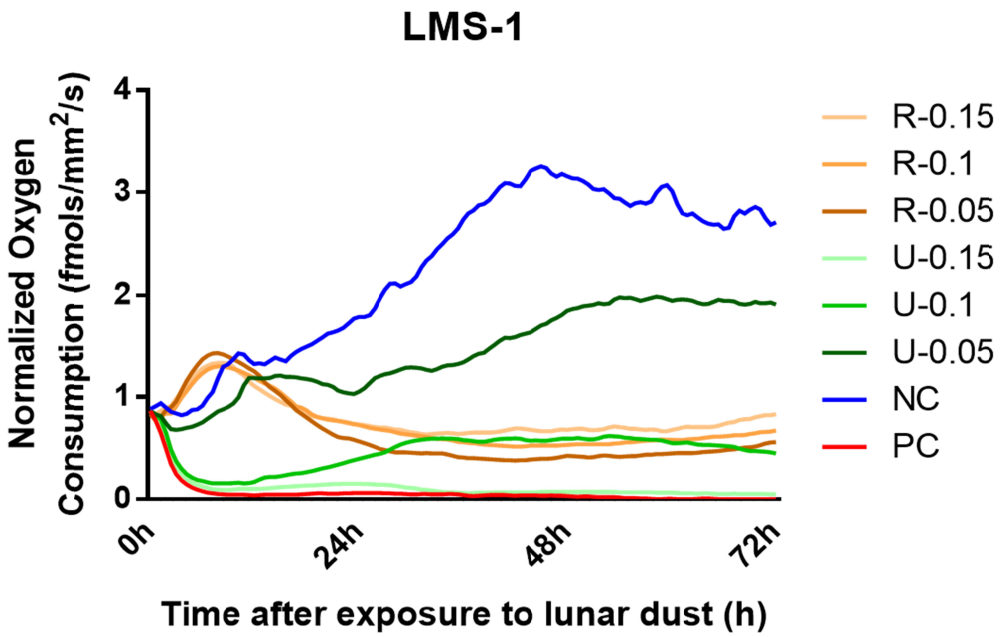

Figure 6. Normalized oxygen consumption rate in simulant-exposed cells. The RESIPHER instrument (LUCID Scientific) measures real-time O_2 consumption by cells in culture. A549 cells were treated with reduced (R) or untreated (U) LMS-1 (n=4) at 0.05, 0.1, or 0.15 mg/cm^2 and O_2 consumption monitored continuously over the next 72h. Negative control (NC): no toxic challenge; positive control (PC): treatment with antimycin A.

3.5 Nuclear DNA Damage from Exposure to Lunar Dust Simulants

In a prior study [*Caston et al.*, 2018], we showed using a PCR-based assay that exposure to other lunar regolith simulants caused damage to DNA in the nucleus. However, the assay for nuclear DNA, with just two copies per cell of the target segment for the assay, is rather noisy compared to that for mitochondrial DNA (with hundreds of copies per cell). We therefore used the "comet assay", which detects DNA breaks by the mobilization of the DNA from the nucleus during electrophoresis (examples in Fig. 7A; see Materials and Methods). That approach revealed DNA damage caused by both simulants, which was substantially enhanced by the reducing treatment of the materials (Fig. 7B). In these experiments, LMS-1 appeared to be somewhat more genotoxic than LHS-1 (Fig. 7B). As seen for mitochondrial DNA

damage (Fig. 3), nuclear DNA is harmed as an early effect of dust exposure.

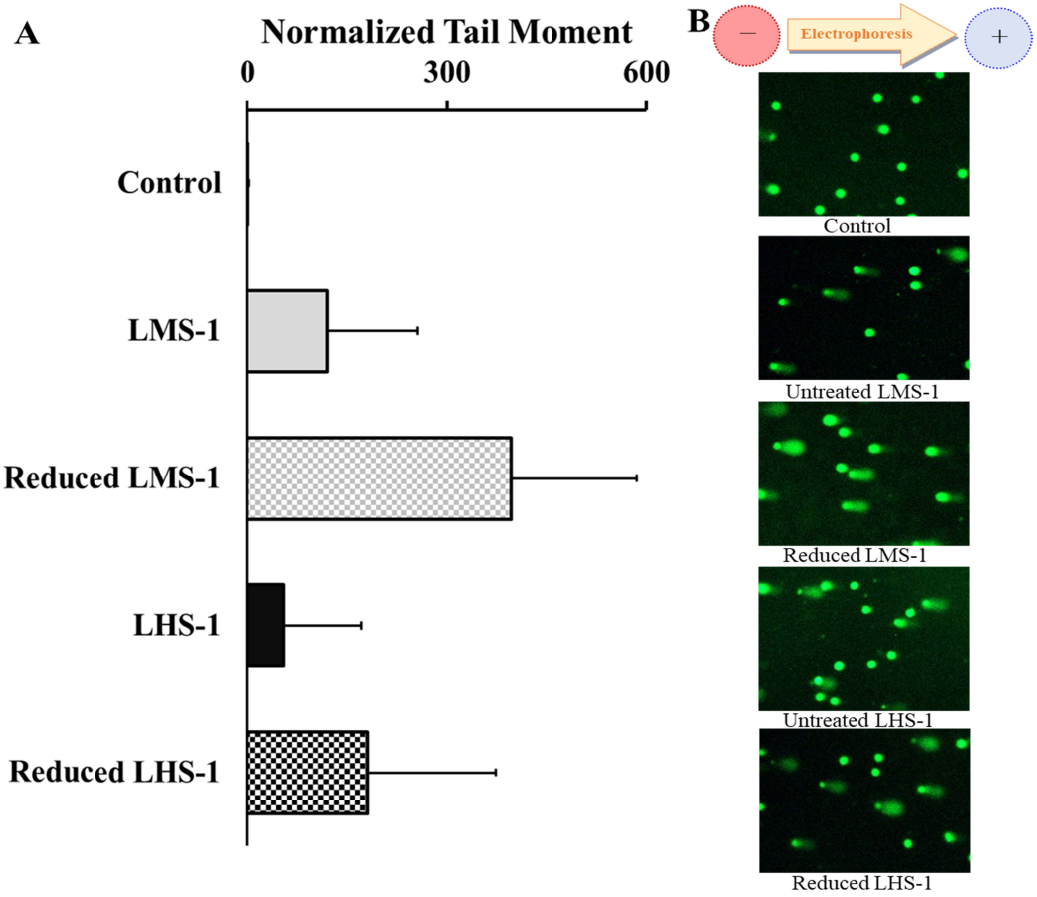

Figure 7. Alkaline comet assay for DNA damage. Freshly-ground LMS-1 or LHS-1 were added at 1 mg/cm^2 to A549 cells for a 1-h exposure, and the samples processed in Materials and Methods. The extent of DNA damage was computed from the length and intensity of the comet-like tails (called the tail moment), shown in **A**. Examples of the fluorescent images are shown in **B**.

4 Discussion

4.1 Summary of Findings

Our new findings can be summarized as follows: 1) the LHS-1 and LMS-1 lunar regolith simulants both appear to be more cytotoxic than the simulants used in our previous studies [*Caston et al.*, 2018]; 2) artificial space weathering to simulate solar wind enhanced all aspects of toxicity for both simulants; 3) there is a significant correlation of toxicity with the iron content of olivine dust; 4) free radicals/ROS are significant components of all aspects of toxicity for both simulants; 5) direct monitoring of cellular O_2 consumption revealed an immediate toxic impact of reduced simulants at levels 10-fold lower than did the other assays; there was some recovery from the lowest level of nonreduced LMS-1, and none at all from higher

nonreduced dust levels or from any level of reduced LMS-1, indicating irreversible mitochondrial damage.

4.2 Enhanced Toxicity of Lunar Dust Simulants with Artificial Space Weathering

The consistent and strong increase in toxicity by simulating the space weathering effects of solar wind indicates that it is likely to be an important aspect of lunar regolith toxicity. Certainly, this observation underscores the need to investigate freshly-collected samples of lunar regolith to test this hypothesis with actual lunar materials. Electron microscopy showed that the reducing treatment produces surface deposits of iron on the particles [*Allen et al.*, 1994], possibly accounting for at least some of the increased toxicity of the reduced materials. Additional studies should address this issue more closely.

4.3 ROS: a Key Component of the Toxicity of Lunar Dust Simulants

While the reducing treatment enhances the ability of simulants to produce •OH radicals in an aqueous environment (Hendrix et al., manuscript submitted), the role of this oxidative activity in cellular damage is uncertain. The broad protective effects of antioxidant supplementation support the view that ROS is an important component of simulant toxicity. However, the amount of direct radical production by the dust appears to be modest [*Hendrix et al.*, 2019], and •OH production by various simulant dusts showed no correlation with toxicity in the lungs of rats [*Lam et al.*, 2022].

4.4 Potential Impact of Long-term Exposure to Lunar Dust Simulants in Human Cells

While the reducing treatment enhances the ability of simulants to produce •OH radicals in an aqueous environment (Hendrix et al., manuscript submitted), the role of this oxidative activity in cellular damage is uncertain. The broad protective effects of antioxidant supplementation support the view that ROS are an important component of simulant toxicity. However, the amount of direct radical production by the dust appears to be modest [*Hendrix et al.*, 2019], and •OH production by various simulant dusts showed no correlation with toxicity in the lungs of rats [*Lam et al.*, 2022]. Mammalian cells themselves actively produce toxic levels of ROS when suitably stimulated, for example by exposure to silica dust [*Skuland et al.*, 2020], titanium oxide [*Skocaj et al.*, 2011], or other fine metallic dust [*Cambre et al.*, 2020], which can continue after the initial exposure [*Lam et al.*, 2022; *Pohlen et al.*, 2022]. Particles that enter deeply into the lungs and lodge in the alveoli can cause persistent local inflammation, which is associated with a strong cancer risk [*Merget et al.*, 2002; *Ovrevik et al.*, 2002; *Saraf et al.*, 1999; *Skuland et al.*, 2020; *Xu et al.*, 2020]. If lunar dust similarly causes persistent local ROS generation in the lungs, which seems likely in view of what we know, that would constitute a significant long-term health risk for lunar explorers. Damage leading to long-term health consequences is also possible for other tissues (e.g., the eyes) [*Braddock*, 2021; *Heiken et al.*, 1991; *James and Kahn-Mayberry*, 2009; *Lam et al.*, 2022].

Damage to mitochondria, which are vital organelles in the cell, and disruption of mitochondrial energy production, was documented in multiple ways in this study. In addition to acting as a source of persistent inflammatory ROS, mitochondria can trigger other cell signaling pathways, including those that activate cell death

mechanisms [*Mittal et al.*, 2014; *Ryter et al.*, 2007; *Van Houten et al.*, 2016]. Consequently, tissue damage would be a significant short-term risk for lunar regolith exposure, via tissue loss or derangement in the exposed organs. Engineering should be able to mitigate much of the short-term risk by minimizing explorer exposure to Moon dust. However, incidental or accidental exposure is hard to prevent completely [*Braddock*, 2021; *Cain*, 2010; *Winterhalter et al.*, 2020]. Assays at low exposure levels would be helpful in this regard in establishing levels where there is no detectable impact. We have made a step in that direction by showing that the RESIPHER device enables us to detect substantial disruption of mitochondria at dust exposure levels 10-fold lower than can be detected with other assays.

4.5 Prospective Health Hazards for Artemis Astronauts

The possible health hazards of lunar dust exposure may seem minor in comparison with other likely risks for Artemis explorers [*Pohlen et al.*, 2022]. However, such materials may also have a longer-term impact [*Lam et al.*, 2022], which should be offset in favor of astronaut health. One way by which the research we present contributes is to point the way for the development of portable instruments to use for reporting dust toxicity during exploration of the Moon's surface. For example, improvements to lung-on-a-chip approaches [*Skuland et al.*, 2020; *Xu et al.*, 2020; *Zhang et al.*, 2018] should provide increasingly useful bioassay devices that lunar explorers can use for their own protection.

Acknowledgments

We thank the laboratories of Dr. Daniel Bogenhagen, Dr. Hyungjin Kim, and Dr. Stella Tsirka for providing helpful technical advice. We are grateful to Dr. Chioma Okeoma for allowing us to use her BioTek Lionheart Imager, and to Dr. Markus Seeliger for the use of the plate reader. This work was supported by a grant from NASA (NNA114AB04A; P.I. T. Glotch, Stony Brook University).

Conflict of Interest

The authors all declare no conflict of interest concerning this work.

References

Allen, C. C., R. V. Morris, and D. S. Mckay (1994), Experimental Reduction of Lunar Mare Soil and Volcanic Glass, J Geophys Res-Planet, 99(E11), 23173-23185, doi: Doi 10.1029/94je02321.

Ates, B., L. Abraham, and N. Ercal (2008), Antioxidant and free radical scavenging properties of N-acetylcysteine amide (NACA) and comparison with N-acetylcysteine (NAC), Free Radic Res, 42(4), 372-377, doi: 10.1080/10715760801998638.

Ayala-Torres, S., Y. Chen, T. Svoboda, J. Rosenblatt, and B. Van Houten (2000), Analysis of gene-specific DNA damage and repair using quantitative polymerase chain reaction, Methods, 22(2), 135-147, doi: 10.1006/meth.2000.1054.

Braddock, M. (2021), Hazards of Lunar Regolith for Respiratory, Central Nervous System, Cardiovascular and Ocular Function, The Human Factor in the Settlement of the Moon: An Interdisciplinary Approach, 141-157.

Cain, J. R. (2010), Lunar dust: The Hazard and Astronaut Exposure Risks, Earth Moon Planets, 107(1), 107-125, doi: 10.1007/s11038-010-9365-0.

Cambre, M. H., et al. (2020), Cytotoxicity of NiO and Ni(OH)(2) Nanoparticles Is Mediated by Oxidative Stress-Induced Cell Death and Suppression of Cell Proliferation, Int J Mol Sci, 21(7), doi: 10.3390/ijms21072355.

Caston, R., K. Luc, D. Hendrix, J. A. Hurowitz, and B. Demple (2018), Assessing Toxicity and Nuclear and Mitochondrial DNA Damage Caused by Exposure of Mammalian Cells to Lunar Regolith Simulants, Geohealth, 2(4), 139-148, doi: 10.1002/2017GH000125.

Furda, A., J. H. Santos, J. N. Meyer, and B. Van Houten (2014), Quantitative PCR-based measurement of nuclear and mitochondrial DNA damage and repair in mammalian cells, Methods Mol Biol, 1105, 419-437, doi: 10.1007/978-1-62703-739-6_31.

Gondhalekar, M., C. Parks, N. Shetty, and B. Wang (2020), Mitigation and Prevention of Lunar Dust on NASA Artemis xEMU Spacesuits, edited, pp. 6-8.

Gyori, B. M., G. Venkatachalam, P. S. Thiagarajan, D. Hsu, and M. V. Clement (2014), OpenComet: an automated tool for comet assay image analysis, Redox Biol, 2, 457-465, doi: 10.1016/j.redox.2013.12.020.

Heiken, G., D. Vaniman, and B. M. French (1991), Lunar sourcebook : a user's guide to the moon, 121-337 pp., Cambridge University Press, Cambridge England ; New York.

Hendrix, D. A., S. T. Port, J. A. Hurowitz, and M. A. Schoonen (2019), Measurement of OH* Generation by Pulverized Minerals Using Electron Spin Resonance Spectroscopy and Implications for the Reactivity of Planetary Regolith, Geohealth, 3(1), 28-42, doi: 10.1029/2018GH000175.

Hendrix, D. A., J. A. Hurowitz, T. D. Glotch, and M. A. A. Schoonen (2021), Olivine Dissolution in Simulated Lung and Gastric Fluid as an Analog to the Behavior of Lunar Particulate Matter Inside the Human Respiratory and Gastrointestinal Systems, Geohealth, 5(11), e2021GH000491, doi: 10.1029/2021GH000491.

Hessel, P., G. Sluis-Cremer, E. Hnizdo, M. Faure, R. G. Thomas, and F. Wiles (1988), Progression of silicosis in relation to silica dust exposure, in Inhaled Particles VI, edited, pp. 689-696, Elsevier.

Hnizdo, E., and V. Vallyathan (2003), Chronic obstructive pulmonary disease due to occupational exposure to silica dust: a review of epidemiological and pathological evidence, Occup Environ Med, 60(4), 237-243, doi: 10.1136/oem.60.4.237.

Hnizdo, E., J. Murray, and S. Klempman (1997), Lung cancer in relation to exposure to silica dust, silicosis and uranium production in South African gold miners, Thorax, 52(3), 271-275, doi: 10.1136/thx.52.3.271.

Hsu, H. T., Y. T. Tseng, W. J. Wong, C. M. Liu, and Y. C. Lo (2018), Resveratrol prevents nanoparticles-induced inflammation and oxidative stress via downregulation of PKC-alpha and NADPH oxidase in lung epithelial A549 cells, BMC Complement Altern Med, 18(1), 211, doi: 10.1186/s12906-018-2278-6.

Hu, G., X. Cun, S. Ruan, K. Shi, Y. Wang, Q. Kuang, C. Hu, W. Xiao, Q. He, and H. Gao (2016), Utilizing G2/M retention effect to enhance tumor accumulation of active targeting nanoparticles, Sci Rep, 6(1), 27669, doi: 10.1038/srep27669.

James, J. T., and N. Kahn-Mayberry (2009), Risk of adverse health effects from lunar dust exposure, in The Human Research Program Evidence Book, NASA-SP-2009-3045., edited, pp. 317-330, NASA.

Kowaltowski, A. J., N. C. de Souza-Pinto, R. F. Castilho, and A. E. Vercesi (2009), Mitochondria and reactive oxygen species, Free Radic Biol Med, 47(4), 333-343, doi: 10.1016/j.freeradbiomed.2009.05.004.

Laboratories, C. S. H. (2006), Hank's Balanced Salt Solution (HBSS) without Phenol Red, in *Cold Spring Harbor Protocols*, edited, p. pdb.rec548.

Lam, C. W., et al. (2022), Comparative pulmonary toxicities of lunar dusts and terrestrial dusts (TiO(2) & SiO(2)) in rats and an assessment of the impact of particle-generated oxidants on the dusts' toxicities, Inhal Toxicol, 34(3-4), 51-67, doi: 10.1080/08958378.2022.2038736.

Linnarsson, D., J. Carpenter, B. Fubini, P. Gerde, L. L. Karlsson, D. J. Loftus, G. K. Prisk, U. Staufer, E. M. Tranfield, and W. van Westrenen (2012), Toxicity of lunar dust, Planetary and Space Science, 74(1), 57-71, doi: 10.1016/j.pss.2012.05.023.

Loftus, D. J., E. M. Tranfield, J. C. Rask, and C. McCrosssin (2008), The chemical reactivity of lunar dust relevant to human exploration of the Moon, edited, pp. 2-4, NASA Ames Research Center, USA.

Medina-Reyes, E. I., L. Bucio-Lopez, V. Freyre-Fonseca, Y. Sanchez-Perez, C. M. Garcia-Cuellar, R. Morales-Barcenas, J. Pedraza-Chaverri, and Y. I. Chirino (2015), Cell cycle synchronization reveals greater G2/M-phase accumulation of lung epithelial cells exposed to titanium dioxide nanoparticles, Environ Sci Pollut Res Int, 22(5), 3976-3982, doi: 10.1007/s11356-014-3871-y.

Merget, R., T. Bauer, H. U. Kupper, S. Philippou, H. D. Bauer, R. Breitstadt, and T. Bruening (2002), Health hazards due to the inhalation of amorphous silica, Archives of Toxicology, 75(11-12), 625-634, doi: 10.1007/S002040100266.

Mitsopoulos, P., and Z. E. Suntres (2011), Protective Effects of Liposomal N-Acetylcysteine against Paraquat-Induced Cytotoxicity and Gene Expression, J Toxicol, 2011, 808967, doi: 10.1155/2011/808967.

Mittal, M., M. R. Siddiqui, K. Tran, S. P. Reddy, and A. B. Malik (2014), Reactive oxygen species in inflammation and tissue injury, Antioxid Redox Signal, 20(7), 1126-1167, doi: 10.1089/ars.2012.5149.

Muruzabal, D., A. Collins, and A. Azqueta (2021), The enzyme-modified comet assay: Past, present and future, Food Chem Toxicol, 147, 111865, doi: 10.1016/j.fct.2020.111865.

Nowsheen, S., F. Xia, and E. S. Yang (2012), Assaying DNA damage in hippocampal neurons using the comet assay, J Vis Exp(70), e50049, doi: 10.3791/50049.

Ovrevik, J., M. Låg, R. Hetland, P. Schwarze, and M. Refsnes (2002), Stone Particle-induced Interleukin-6 and -8 Release Involves Activation of MAP Kinases and Tyrosine Kinases, The Annals of Occupational Hygiene, 46, doi: 10.1093/annhyg/46.suppl_1.390.

Pohlen, M., D. Carroll, G. K. Prisk, and A. J. Sawyer (2022), Overview of lunar dust toxicity risk, NPJ Microgravity, 8(1), 55, doi: 10.1038/s41526-022-00244-1.

Ryter, S. W., H. P. Kim, A. Hoetzel, J. W. Park, K. Nakahira, X. Wang, and A. M. Choi (2007), Mechanisms of cell death in oxidative stress, Antioxid Redox Signal, 9(1), 49-89, doi: 10.1089/ars.2007.9.49.

Saraf, A., L. Larsson, B. M. Larsson, K. Larsson, and L. Palmberg (1999), House dust induces IL-6 and IL-8 response in A549 epithelial cells, Indoor Air, 9(4), 219-225, doi: 10.1111/j.1600-0668.1999.00002.x.

Skocaj, M., M. Filipic, J. Petkovic, and S. Novak (2011), Titanium dioxide in our everyday life; is it safe?, Radiology and oncology, 45(4), 227.

Skuland, T., M. Lag, A. C. Gutleb, B. C. Brinchmann, T. Serchi, J. Ovrevik, J. A. Holme, and M. Refsnes (2020), Pro-inflammatory effects of crystalline- and nano-sized non-crystalline silica particles in a 3D alveolar model, Part Fibre Toxicol, 17(1), 13, doi: 10.1186/s12989-020-00345-3.

Strober, W. (2001), Trypan blue exclusion test of cell viability, Curr Protoc Immunol, Appendix 3, Appendix 3B, doi: 10.1002/0471142735.ima03bs21.

Tice, R. R., E. Agurell, D. Anderson, B. Burlinson, A. Hartmann, H. Kobayashi, Y. Miyamae, E. Rojas, J. C. Ryu, and Y. F. Sasaki (2000), Single cell gel/comet assay: guidelines for in vitro and in vivo genetic toxicology testing, Environ Mol Mutagen, 35(3), 206-221, doi: 10.1002/(sici)1098-2280(2000)35:3<206::aid-em8>3.0.co;2-j.

Van Houten, B., S. E. Hunter, and J. N. Meyer (2016), Mitochondrial DNA damage induced autophagy, cell death, and disease, Front Biosci (Landmark Ed), 21(1), 42-54, doi: 10.2741/4375.

Wagner, S. A. (2006), The Apollo experience lessons learned for constellation lunar dust management, NASA Technical Publication TP-2006-213726. Washington, DC: National Aeronautics and Space Administration.

Winterhalter, D., J. S. Levine, R. L. Kerschmann, and T. K. Brady (2020), Lunar Dust and Its Impact on Human Exploration: A NASA Engineering and Safety Center (NESC) Workshop*Rep.*

Wojtala, A., M. Bonora, D. Malinska, P. Pinton, J. Duszynski, and M. R. Wieckowski (2014), Methods to monitor ROS production by fluorescence microscopy and fluorometry, Methods Enzymol, 542, 243-262, doi: 10.1016/B978-0-12-416618-9.00013-3.

Xu, C., M. Zhang, W. Chen, L. Jiang, C. Chen, and J. Qin (2020), Assessment of Air Pollutant PM2.5 Pulmonary Exposure Using a 3D Lung-on-Chip Model, ACS Biomater Sci Eng, 6(5), 3081-3090, doi: 10.1021/acsbiomaterials.0c00221.

Zhang, M., C. Xu, L. Jiang, and J. Qin (2018), A 3D human lung-on-a-chip model for nanotoxicity testing, Toxicol Res (Camb), 7(6), 1048-1060, doi: 10.1039/c8tx00156a.

569 Table 1

570

571 *Forward and reverse primers used in the quantitative PCR assay*

Primers used	Sequence (5'→3')
Human mitochondrial long, sense strand	TCTAAGCCTCCTTATTCGAGCCGA
Human mitochondrial long, antisense strand	TTTCATCATGCGGAGATGTTGGATGG
Human mitochondrial short, sense strand	CCCCACAAACCCCATTACTAAACCCA
Human mitochondrial short, antisense strand	TTTCATCATGCGGAGATGTTGGATGG

572

Table 2

Cell-killing rates normalized to dust surface area

Lunar dust simulant	Cell-killing by 0.5 mg/cm^2 dust (% per h)		Total dust surface area (cm^2)	Cell killing rate (% per h per cm^2 of surface)	
	No NAC	NAC supplemented		No NAC	NAC supplemented
LMS-1	48	25	430	0.11	0.06
Reduced LMS-1	71	41	200	0.36	0.21
LHS-1	60	48	280	0.21	0.17
Reduced LHS-1	82	66	160	0.51	0.41

573

574 Table 3

575

576 *Composition of LHS-1 and LMS-1 (weight percent)*

577

LHS-1		LMS-1	
Plagioclase	74.4%	Pyroxene	32.8%
Glass	24.2%	Glass	24.5%
Basalt	0.5%	Plagioclase	19.8%
Ilmenite	0.4%	Olivine	11.1%
Pyroxene	0.3%	Basalt	7.5%
Olivine	0.2%	Ilmenite	4.3%

578